A nonlinear model of noise-sustained structures in subcritical systems

Edgar Knobloch

University of California, Berkeley, CA 94720, USA

knobloch@berkeley.edu

http://tardis.berkeley.edu

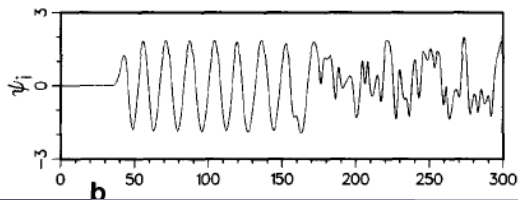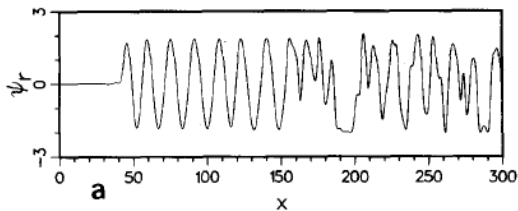joint work with Daniele Avitabile, Mathieu Desroches and Martin Krupa

KITP, Santa Barbara, 12 January 2017

Noise-sustained structures

Deissler (Phys D 25, 233 (1987); PLA 120, 334 (1987)) studied the complex Ginzburg-Landau equation

$$\psi_t = a\psi - v_g\psi_x + b\psi_{xx} - c|\psi|^2\psi, \qquad x \in [0, \infty).$$

For $0 < a_r < b_r v_g^2/4|b|^2$ the state $\psi = 0$ is convectively unstable:
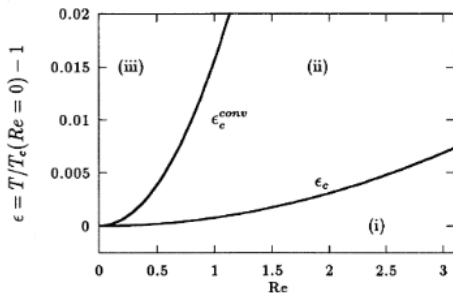
Convective vs absolute instability

FIG. 2. Convective vs absolute instability for axisymmetric perturbations. The basic flow state is absolutely stable in the region (i) below the curve ϵ_c, convectively unstable in the region (ii) between the curves ϵ_{conv}^c and ϵ_c, and absolutely unstable in the region (iii) above the curve ϵ_{conv}^c. Here the radius ratio is $\eta = 0.75$ but the curves practically do not vary with η in the plot range shown.

Recktenwald et al., PRE 48, 4444 (1993): Taylor vortices with axial through-flow

The model

We study the model problem (Chomaz & Couairon: PF 11, 2977 (1999)):

$$A_t = A_{xx} - (U - \alpha A^2)A_x + \mu A - A^3, \qquad x \in [0, L].$$

Here $A(x, t)$ is a real field, and $U > 0$ and $\alpha > 0$ are real parameters.

On the real line the trivial state $A = 0$ is convectively unstable for $\mu > 0$ and absolutely unstable for $\mu > \mu_a \equiv U^2/4$.

The basic question is what happens in a finite domain $0 \leq x \leq L$?

With $A(0, t) = A(L, t) = 0$ there is no instability until $\mu = \mu_g \approx \mu_a + O(L^{-2})$ at which point there is a subcritical bifurcation to a branch of stationary global modes of the system with $\mathcal{O}(\sqrt{\mu})$ amplitude. These states are present for $\mu \geq \mu_*$, $0 < \mu_* < \mu_g$.

We shall be interested in the regime with $U \gg 1$ (strong advection) with $0 < |A(0, t)| = \eta \ll 1$, with η either constant or time-dependent. The remaining parameters are all $O(1)$. In all cases $A(L, t) = 0$.
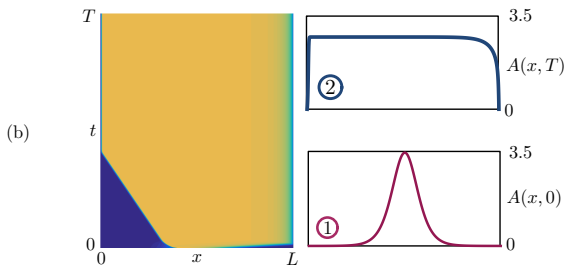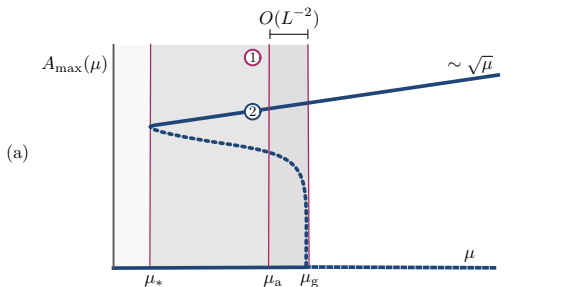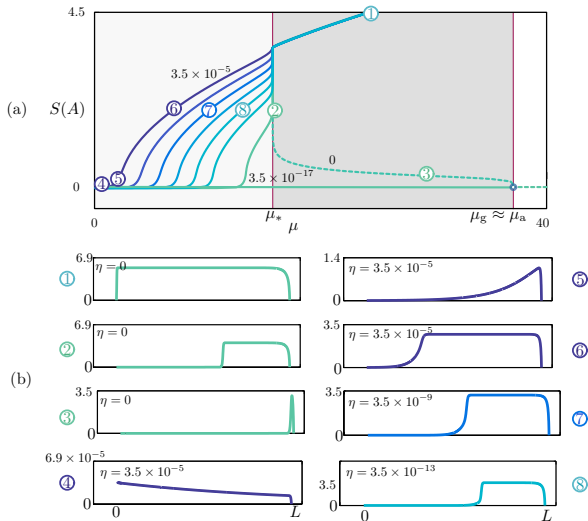
(a) Bifurcation diagram of steady states satisfying $A(0,t) = A(L,t) \equiv 0$.

(b) Time simulation with $\mu = 7.4 < \mu_a$, $\alpha = 5$, $U = 12$.
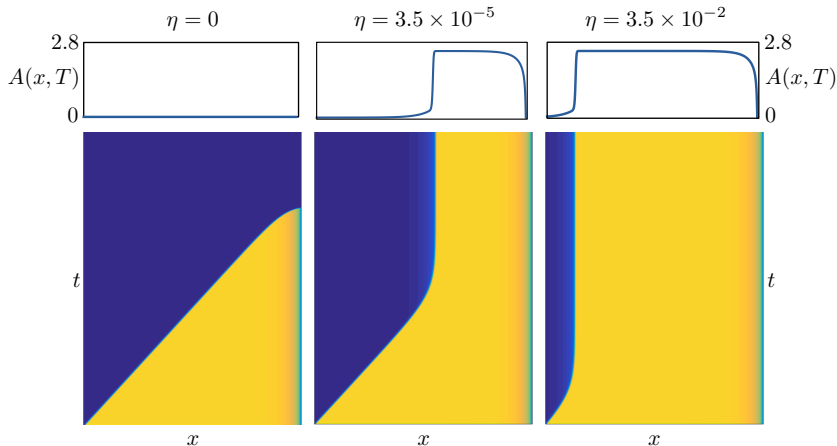
Time simulation with $\mu = 7.4 < \mu_{\mathrm{a}}$, $\alpha = 5$, $U = 12$ and $A(0,t) = \eta$. (a) $\eta = 0$. (b) $\eta = 3.5 \times 10^{-5}$. (c) $\eta = 3.5 \times 10^{-2}$. In all cases $A(L,t) = 0$.

(a) Branches of steady states for $\alpha = 2$, $U = 12$, $L = 10\pi$ in terms of $S(A) \equiv -\mathrm{sgn}A'(L)\|A\|_2$ for $A(0, t) = \eta \in [0, 3.5 \times 10^{-5}]$. (b) The solution profiles $A(x)$, $x \in [0, L]$. The states in $\mu < \mu_*$ ($\mu > \mu_*$) originate in the convective (absolute) instability of $A = 0$.

The scaled model

We suppose that $U^{-2} \equiv \epsilon \ll 1$ and rescale the equations as follows:

$$A = \epsilon^{-1/4}A', \qquad x = \epsilon^{1/2}x', \qquad t = \epsilon t'$$

and suppose that A', x' and t' are $O(1)$. Thus $L = \epsilon^{1/2}\ell$, where ℓ is formally $O(1)$ but is large compared to the scale of the front. These scalings all follow from the observation that rapid advection will be balanced by diffusion only on appropriately small spatial scales and that evolution will then inevitably take place on the short, advective, time scale. Dropping primes, we have:

$$A_t = A_{xx} - (1 - \alpha A^2)A_x + \epsilon\mu A - \sqrt{\epsilon}A^3, \qquad (x, t) \in [0, \ell] \times [0, \infty).$$

This equation is to be solved subject to the Dirichlet boundary conditions

$$A(0, t) = \eta, \qquad A(\ell, t) = 0, \qquad t \in [0, \infty).$$

Steady states of the scaled model

The steady states of the PDE model constitute a **spatial** van der Pol oscillator. We set $z_1 = A$ and use the Liénard transformation $z_2 = -A' + A - (\alpha/3)A^3$ to obtain the first-order BVP (system A)

$$z_1' = -z_2 + z_1 - \frac{\alpha}{3}z_1^3$$
$$z_2' = \sqrt{\epsilon}(\sqrt{\epsilon}\mu z_1 - z_1^3)$$
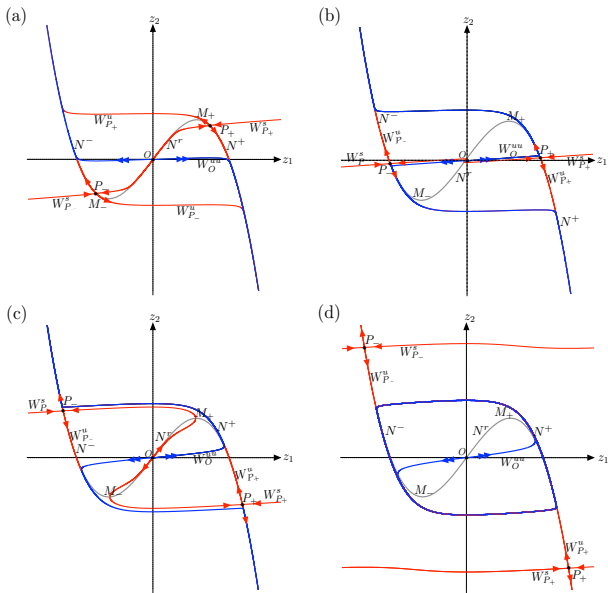$$z_1(0) = \eta, \quad z_1(\ell) = 0.$$

The slow-fast structure of this problem makes it amenable to analysis. Stability of solutions within this ODE system represents **spatial** stability and must be distinguished from **temporal stability** which is determined from the eigenvalues λ of the nonautonomous linear BVP

$$\mathcal{L}[A(x)]\psi = \lambda\psi,$$

where

$$\mathcal{L}[A(x)] := \partial_x^2 - (1 - \alpha A^2)\partial_x + 2\alpha A\partial_x A + \epsilon\mu - 3\sqrt{\epsilon}A^2$$

and $\psi(0) = \psi(\ell) = 0$.

The phase plane for $\epsilon = 1/144$, $\alpha = 5$, and (a) $\mu = 4$ (region 1), (b) $\mu = 7$ (region 2), (c) $\mu = 10$ (region 2), (d) $\mu = 13$ (region 3).

Orbit flip bifurcation

This takes place when $W^s(P_+)$ coincides with the *strong unstable manifold* of O, denoted by $W^{uu}(O)$. This occurs when $\mu = \mu_* = 3\alpha^{-1}(U - 3\alpha^{-1}) \approx 3/(\alpha\sqrt{\epsilon})$. For $\mu > \mu_*$ the separatrix $W^s(P_+)$ must be below $W^{uu}(O)$. Hence, continued backwards in 'time', it must intersect the z_2 axis at some $z_{2,s} < 0$. It follows that for each $z_2 \in (0, z_{2,s})$ there exists $\ell > 0$ such that the BVP has a solution with this choice of ℓ and $z_2(0) = z_2$. Note that $\ell \to \infty$ both as $z_2(0)$ tends to 0 and to $z_{2,s}$. It follows that for ℓ large enough there exist at least two solutions of the BVP for the same ℓ, one with z_2 close to 0 and one with z_2 close to $z_{2,s}$. The solution with $z_2(0) \approx 0$ spends a long 'time' near O since O is a fixed point, which implies that its L_2 norm is small. The solution starting near $z_{2,s}$ spends a long 'time' near P_+ for the same reason and its L_2 norm is therefore large. As μ approaches μ_* from above these two solutions approach each other and the solution with the small L_2 norm develops a longer segment near P_+, implying rapid growth of the L_2 norm. This explains the quasi-vertical segment of the solution branch near $\mu = \mu_*$. A second orbit flip takes place when $W^s(P_+)$ coincides with the other branch of $W^{uu}(O)$.
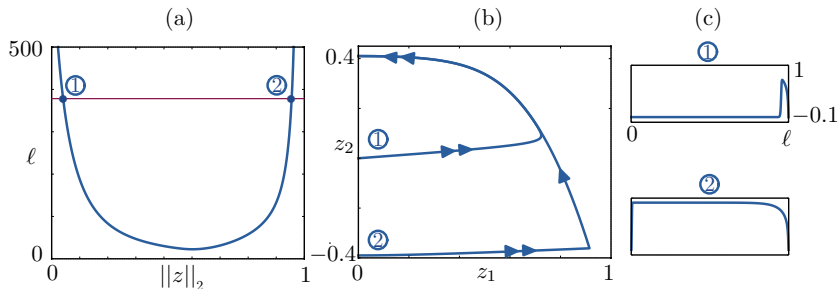
(a) Solution branch obtained by varying ℓ for $\epsilon = 1/144$, $\mu = 10$, $\alpha = 5$ and $\eta = 0$. Two solutions are found for $\ell = 377$ (straight line), and these are shown as trajectories in the spatial phase plane (z_1, z_2) (panel (b)) and as space-dependent stationary states $A(x)$ of the PDE (panel (c)).
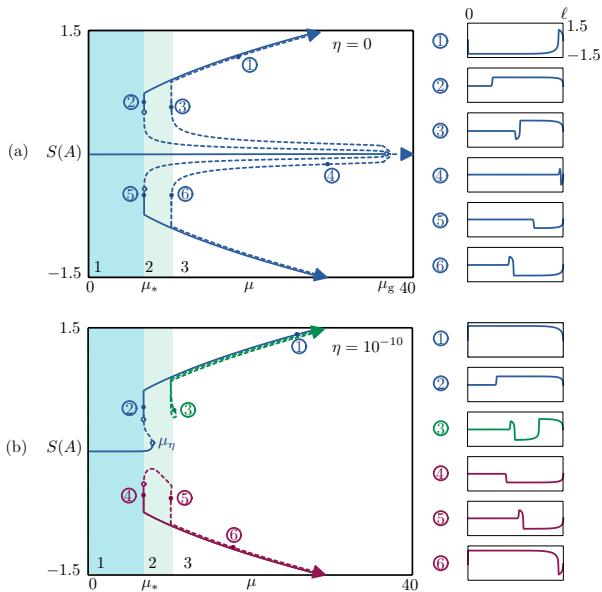
Bifurcation diagram for $\epsilon = 1/144$, $\alpha = 5$, and (a) $\eta = 0$, (b) $\eta = 10^{-10}$, represented using the solution measure $S(A) = -\mathrm{sgn}A'(\ell)\|A\|_2$.
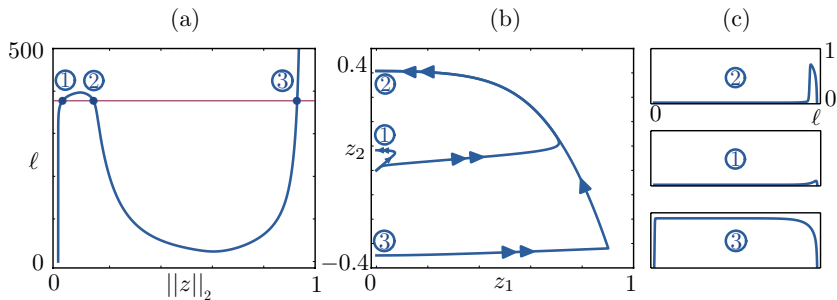
(a) Solution branch of system A obtained by varying ℓ for fixed $\mu = 10$, $\alpha = 5$ and $\eta = 10^{-13}$. Three solutions are found for $\ell = 377$, shown in panels (b) and (c).
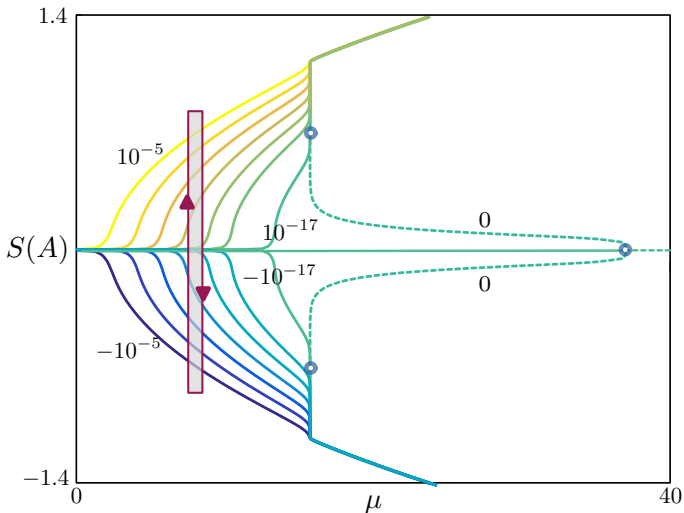
Branches of steady states with $\alpha=2$ and $\eta \in [-10^{-5}, 10^{-5}]$ with a superposed cycle (in red) showing changes in the solution amplitude when η oscillates quasistatically in time with $O(10^{-5})$ amplitude and mean $\eta = 0$.
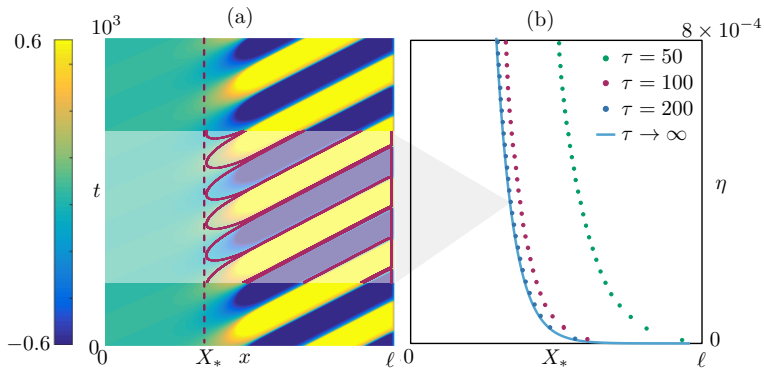
(a) Location X_* of time-periodic fronts with time-periodic inlet boundary condition $A(0, t) = \eta \sin(2\pi t/\tau)$; such fronts are sustained entirely by the small amplitude modulation in $A(0, t)$ (here $\mu = 6.1$, $\eta = 4 \times 10^{-4}$, $\tau = 200$). The red lines in the central part are the contour lines $A(x, t) = \pm 0.1$. (b) The front location X_* for various values η and τ (dots). The curve marked $\tau \to \infty$ represents the front location in the steady state profiles.

Front location

In order to quantify the position of the front, we monitor the level sets of $A(x, t)$ as t varies:

$$X_* = \min_{t \in [0, T]} \{x \in [0, \ell] \colon |A(x, t)| = 0.1\}.$$

When $A(0, t) = \eta(\omega)$ with probability distribution p_η the steady solutions of

$$
\begin{aligned}
A_t &= A_{xx} - (1 - \alpha A^2)A_x + \mu A - \sqrt{\epsilon}A^3, & (x, t) \in (0, \ell) \times (0, T), \\
A(0, t, \omega) &= \eta(\omega), \quad A(\ell, t, \omega) = 0, & t \in [0, T], \\
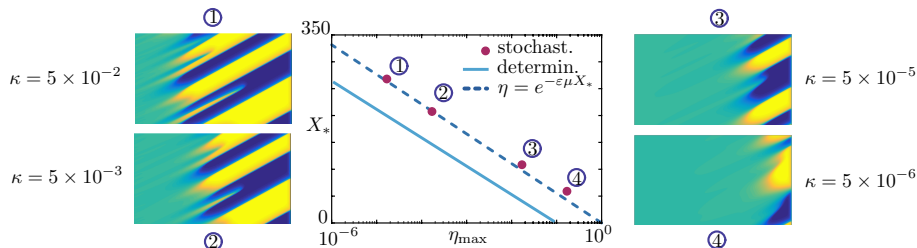A(x, 0, \omega) &= (1 - x/\ell)\eta(\omega), & x \in [0, \ell],
\end{aligned}
$$

generate a probability distribution p_{X_*} of X_*. One can check that $\mathbb{E}[X_*] \to 0$, $\mathrm{var}[X_*] \to 0$ as $\mu \to \mu_*$ from below. For $\mu > \mu_*$ there may be more than one attracting steady state for each event ω.
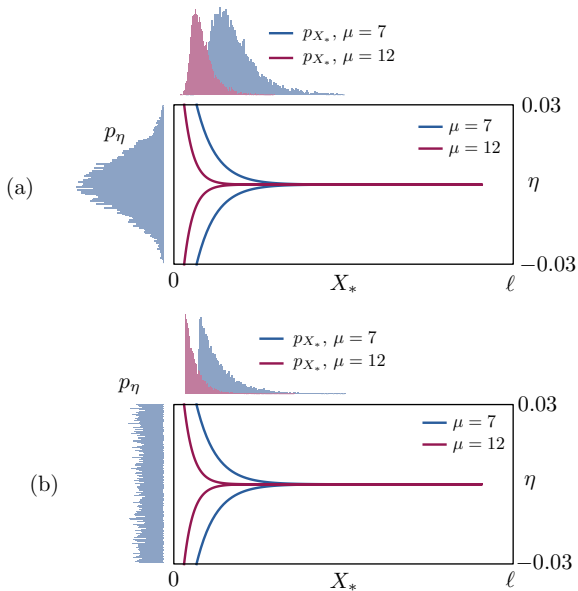
For randomly distributed inlet boundary conditions η with density p_η, the front location X_* is distributed with induced density p_{X_*}.
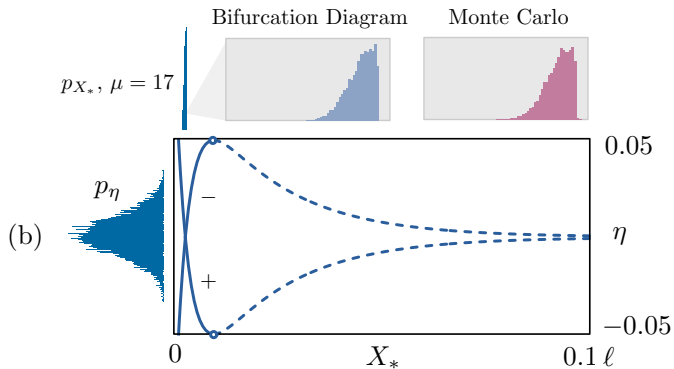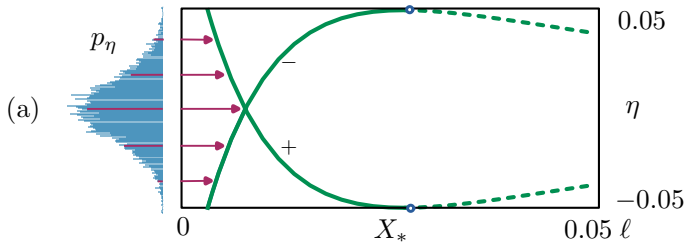
Stochastic simulation

Direct numerical simulations with $A(0, t) = \kappa\eta(t)$, where $\kappa > 0$ and $\eta(t)$ is a Wiener process. We show contour plots of $A(x, t)$ for $(x, t) \in [0, 377] \times [0, 500]$ for $\mu = 6$, $\epsilon = 1/144$ and various values of κ (panels 1–4). For $\kappa = 0$, the only attracting solution is the trivial steady state $A \equiv 0$ but, as the noise is turned on, noise-sustained structures appear. As κ increases so does the maximum inlet amplitude $\eta_{\max} = \max_t |\eta(t)|$, resulting in decreased distance X_* to the noise-sustained front. The deterministic and stochastic setting have a common scaling $\eta = e^{-\epsilon\mu X_*}$.

In fact there are also branches of steady states corresponding to $\eta < 0$:
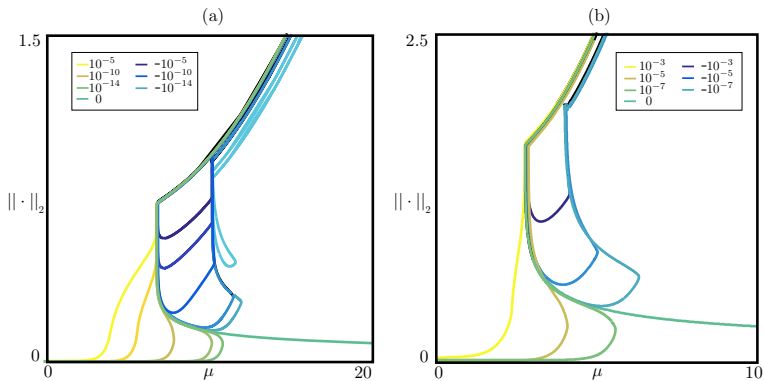

Solution branches for different values of $z_1(0) \equiv \eta$ when $\alpha = 5$, $\epsilon = 1/144$ in system A (panel (a)), and when $\alpha = 1$, $\epsilon = 1/144$ in system B (panel (b)). The panels show branches for $z_1(0) = \eta \neq 0$; these differ in the sign of η and are organized by an orbit-flip bifurcation at $\mu = \mu_*$.
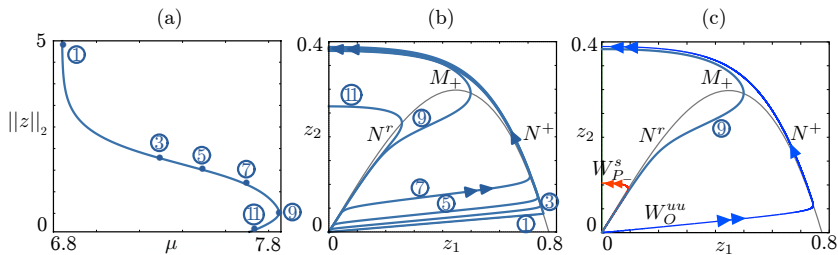
(a) Detail of the type I solution branch of system A with $\eta = 10^{-10}$. (b) Portion of the phase plane showing the trajectories corresponding to the points indicated in (a). (c) Trajectory 9 from (a) and (b), displaying a canard segment, together with some of the invariant manifolds of equilibria of the system present at this value of μ. The point P_+ lies below the z_1 axis.
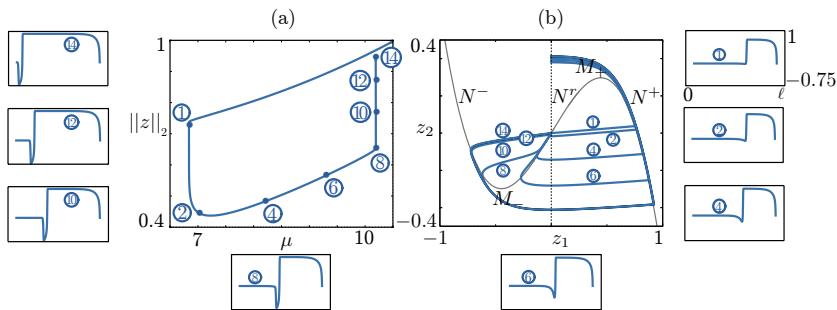
(a) Detail of the type I solution branch of system A with $\eta = -10^{-7}$. (b) Portion of the phase plane showing the trajectories corresponding to the locations indicated in (a). Spatial profiles of the solutions of BVP with $\eta < 0$ corresponding to the trajectories shown in (b) are shown alongside. Here $\mu_* \approx 6.84$ and $\mu_{c+} \approx 10.19$.

(a)   (b)
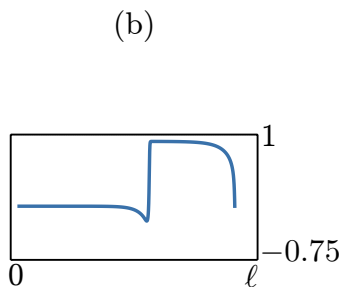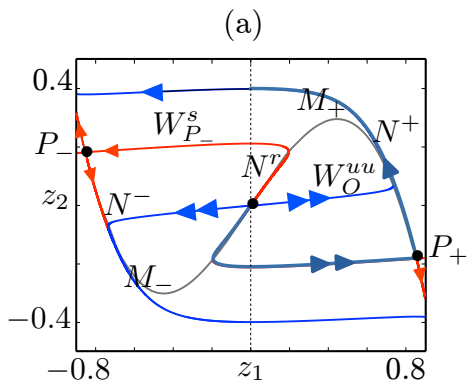
(a) Trajectory 5 (in black) from the previous figure containing a canard segment; also shown is a portion of the phase plane showing the repelling and attracting nullclines as well as stable and unstable manifolds of the three equilibria of the system present at this value of μ. (b) Spatial profile of the corresponding solution to the perturbed BVP with $\eta < 0$.
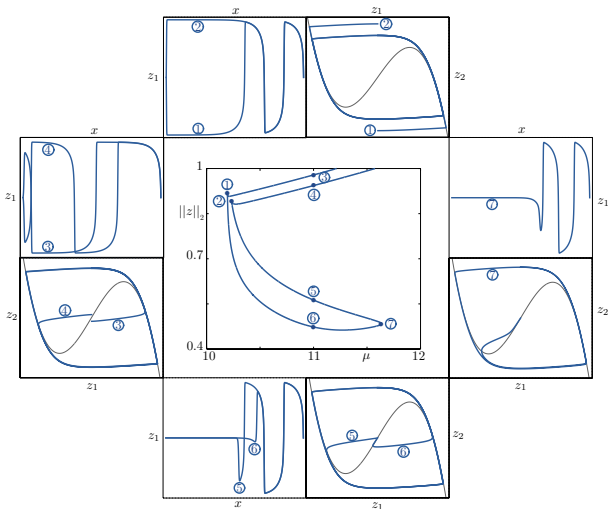
Branch (central panel) corresponding to solutions that make a full turn around O before connecting back to $z_1 = 0$. The central panel shows a zoom of the rightmost branch when $\eta = -10^{-10}$. Side panels show solution profiles in space and in the phase plane at different locations along this branch.
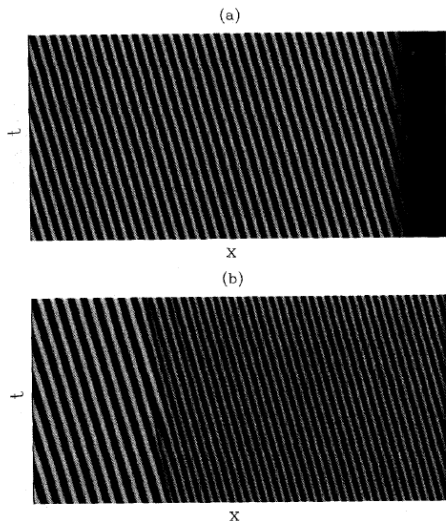
Example: dynamo waves

Fig. 6. Colour-coded space–time plots obtained for the dynamo equations (3) and (4) with $L = 300$ and (a) $D = 8.75$, (b) $D = 15.0$. The domain $(0, L)$ lies along the horizontal axis, with time increasing upward. In (a) the primary front selects the amplitude and wave number of finite amplitude dynamo waves; in (b) a secondary front signals the transition to temporal chaos.

Conclusions

1. The model system displays a high sensitivity to the inlet condition $A(0, t) = \eta$.

2. Numerical continuation of steady states for $\eta \neq 0$ reveals the presence of two types of finite amplitude states, one originating in the convective instability threshold and the other in the absolute instability threshold at $\mu = \mu_{\mathrm{g}}$. The former reveal extreme sensitivity to the value of η and disappear abruptly as $\eta \to 0^+$.

3. The observed sensitivity wrt η finds a natural explanation in the presence of canard segments on solutions of the spatial BVP for the steady states of the model. These results are obtained by recasting the model as a slow-fast system in space and focusing on its steady states subject to $A(0, t) = \eta$, $A(L, t) = 0$. These states correspond to finite length trajectories of a slow-fast spatial-dynamical system of van der Pol type.

4. The stability in time of all steady solutions of the BVP is determined and corroborated using direct numerical simulations.

5. Numerical evidence is presented that demonstrates that the statistics of the front location in the convectively unstable regime can be explained in terms of the properties of the new solution branches in this regime when $\eta \neq 0$.

Conclusions
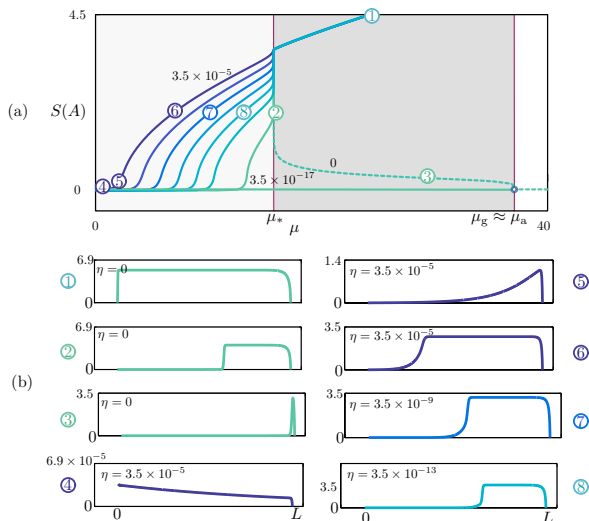
The states in $\mu < \mu_*$ originate in convective instability of $A = 0$ while those in $\mu > \mu_*$ originate in absolute instability of $A = 0$.

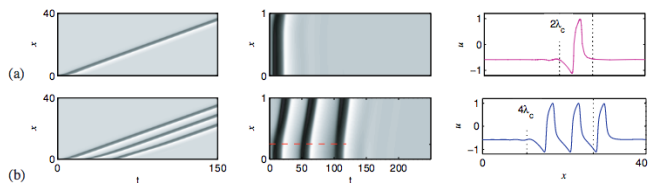# Effect of profile of initial perturbation on pulse generation

Fig. 3: (Color online) Solutions of eqs. (1) at $a_v = 0.5$ with Neumann boundary conditions at $x = 0$, $x = 40$ using different stimuli at $t = 0$: (a) $A = 0.3$, $R = 1$, (b) $A = 0.3$, $R = 0.4$, both for $\Delta = 0.1$. Left panels: space-time plots with x along the vertical axis

Three-component reaction-diffusion system:

$$u_t = u - u^3 - v + Du_{xx}$$
$$v_t = \epsilon_v(u - a_v v - a_w w - a_0)$$
$$w_t = \epsilon_w(u - w) + w_{xx}$$

See Yochelis et al, EPL 83 (2008) 64005 for details

Effect of profile of initial perturbation on pulse generation